Machine Vision and Applications (2015) 26:55–68
DOI 10.1007/s00138-014-0636-z

ORIGINAL PAPER

A self-adaptive matched filter for retinal blood vessel detection

Tapabrata Chakraborti · Dhiraj K. Jha · Ananda S. Chowdhury · Xiaoyi Jiang

Received: 12 November 2013 / Revised: 17 May 2014 / Accepted: 16 July 2014 / Published online: 19 August 2014

Abstract Retinal fundus images are widely studied in medicine for the detection of certain pathologies such as diabetes and glaucoma, the two major reasons for blindness. In this paper, a self-adaptive matched filter for the detection of blood vessels in the retinal fundus images is proposed. In particular, a novel synergistic combination of the vesselness filter with high sensitivity and the matched filter with high specificity is obtained using orientation histogram. Experiments on the publicly available DRIVE database clearly show that the proposed strategy outperforms several existing methods. Comparable performance with some of the state-of-the-art methods has also been obtained on the STARE and CHASE databases.

Keywords Self-adaptive matched filter · Vesselness filter · Orientation histogram · Retinal blood vessel detection

1 Introduction

Study of retinal fundus images has become quite popular for the detection of certain pathologies such as diabetes and glaucoma. This diagnosis is highly important for the early detection and subsequent treatment to prevent the loss of vision, since glaucoma and diabetes are the two major reasons for blindness [1,2]. In order to help the human experts in their screening of numerous samples, computer-aided detection became important to expedite the screening process [3–6]. In this paper, a self-adaptive matched filter, based on the synergistic combination of the vesselness filter [7] and the matched filter [8], is designed using the orientation histogram for solving the challenging problem of retinal blood vessel detection. The purpose of this synergism is to combine the high sensitivity of the vesselness filter with the high specificity of the matched filter. Since the parameters of the matched filter kernel are automatically estimated every time for different inputs, we deem this design as self-adaptive.

The state-of-the-art methods of retinal blood vessel detection can be divided into two major categories, namely, methods which use learning (supervised) and the methods which do not use any form of learning (unsupervised). An exhaustive survey of the existing methods can be found in [9,10]. Methods which employ learning use the training data first. Classification decisions on the test data are taken based on the knowledge acquired during the training process [11]. In sharp contrast, the methods without learning find some inherent patterns of blood vessels in the retinal images that can be used to directly determine whether a particular pixel in the image belongs to a vessel [9]. Though the methods involving learning can provide higher accuracies, they require more time for completion. An even bigger disadvantage of learning based methods is the necessity of training data which may not be available in all the cases. In this paper, a two-step unsupervised method is proposed for the detection of the retinal blood vessels from the fundus images. It has been observed that the vesselness filter [7] yields high sensitivity and low specificity. In contrast, the matched filter [8] provides high specificity and low sensitivity. The proposed method uses orientation histogram to combine the vesselness filter and

T. Chakraborti
Department of Electrical Engineering, Jadavpur University, Kolkata 700032, India

D. K. Jha · A. S. Chowdhury (✉)
Department of Electronics and Telecommunications Engineering, Jadavpur University, Kolkata 700032, India
e-mail: aschowdhury@etce.jdvu.ac.in

X. Jiang
Department of Mathematics and Computer Science, University of Münster, Münster, Germany

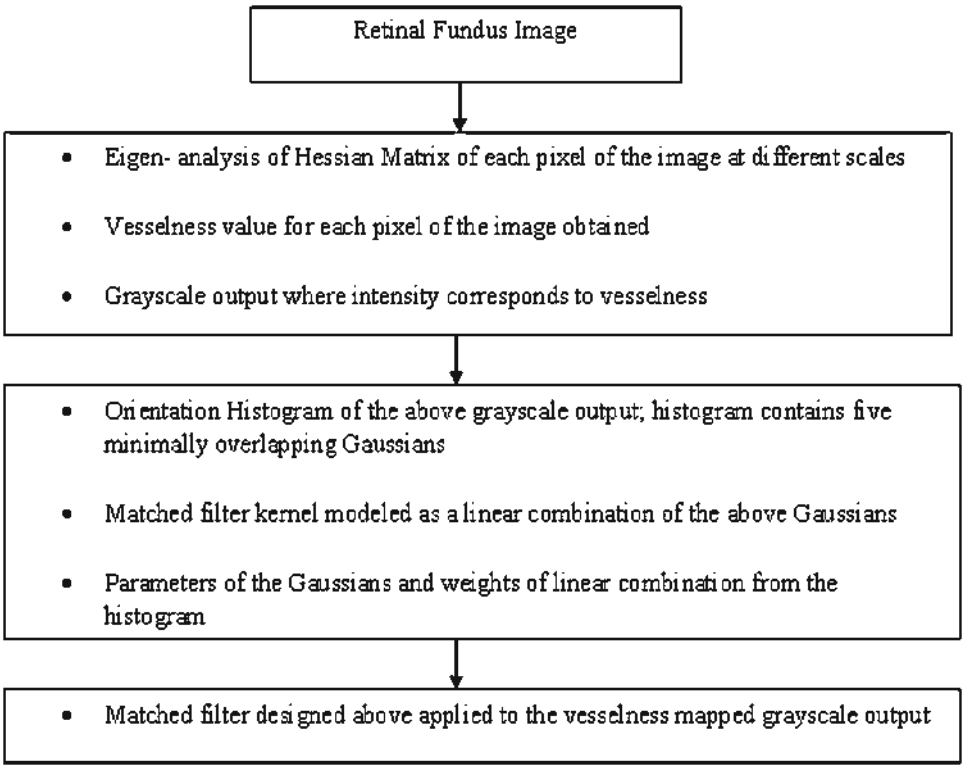

Fig. 1 Flow chart for the proposed method

the matched filter leading to a highly accurate (high sensitivity as well as high specificity) detection. Furthermore, unlike some other unsupervised methods [12], the proposed algorithm uses only a single pass and is hence relatively fast. The vesselness filter [7] based on the eigenvalues of the Hessian matrix is first applied on the input retinal image. Orientation histogram of the output of the vesselness filter is computed next. This orientation histogram is observed to consist of five prominent Gaussians. The kernel of a matched filter [8] is modeled as a linear combination of these five Gaussians and an automated estimation of the relevant parameters of the kernel is performed from the orientation histogram. The matched filter with the above kernel is finally used to improve the detection of the previously obtained vessels.

The rest of the paper is organized as follows: in Sect. 2, some related work along with our contribution is presented. In Sect. 3, the proposed method is described in details. In Sect. 4, the experimental results are shown along with comparisons with several existing approaches. The paper is concluded in Sect. 5 with an outline for the direction of future research.

2 Related work

Due to many important medical applications of the blood vessel segmentation problem in human retinal pathology, extensive research is going on over the years and a wide range of methods, with and without learning, have been proposed. Since the proposed algorithm does not employ any learning strategy, we only review some popular retinal blood vessel detection methods under that category. Chaudhuri et al. [8] proposed a matched filter based method with a single Gaussian kernel centered at the zero angle of rotation for the detection of retinal blood vessels. Chanwimaluang and Fan [13] added entropy thresholding and length filtering to the matched filter in [8] for further improvement of blood vessel detection. Zhang et al. [14] proposed a novel matched filter with first-order derivative of Gaussian for better detection. Cinsdikici and Aydin [15] used a hybrid model of matched filter and ant colony to achieve improved blood vessel detection. Frangi et al. [7] designed a multi-scale vesselness filter function using the eigenvalues of the Hessian matrix of each pixel of the image. The method in [8] yields low sensitivity. The techniques in [13,14], and [15] have improved the matched filter in [8] to some extent. However, none of these methods [13–15] including that of [8] have automated the design of the matched filter kernel based on the individual inputs. The authors in [15] have incorporated the ant colony optimization technique with the matched filter approach. The ant colony optimization being a meta-heuristic iterative process has a high time cost. In [7], Frangi et al. have proposed a vesselness filter which is susceptible to noise and results in low specificity.

In this paper, a non-linear synergistic combination of [7] and [8] is achieved using orientation histogram. The combination improves the specificity of [7] and the sensitivity of [8] to produce a high overall accuracy. The orientation

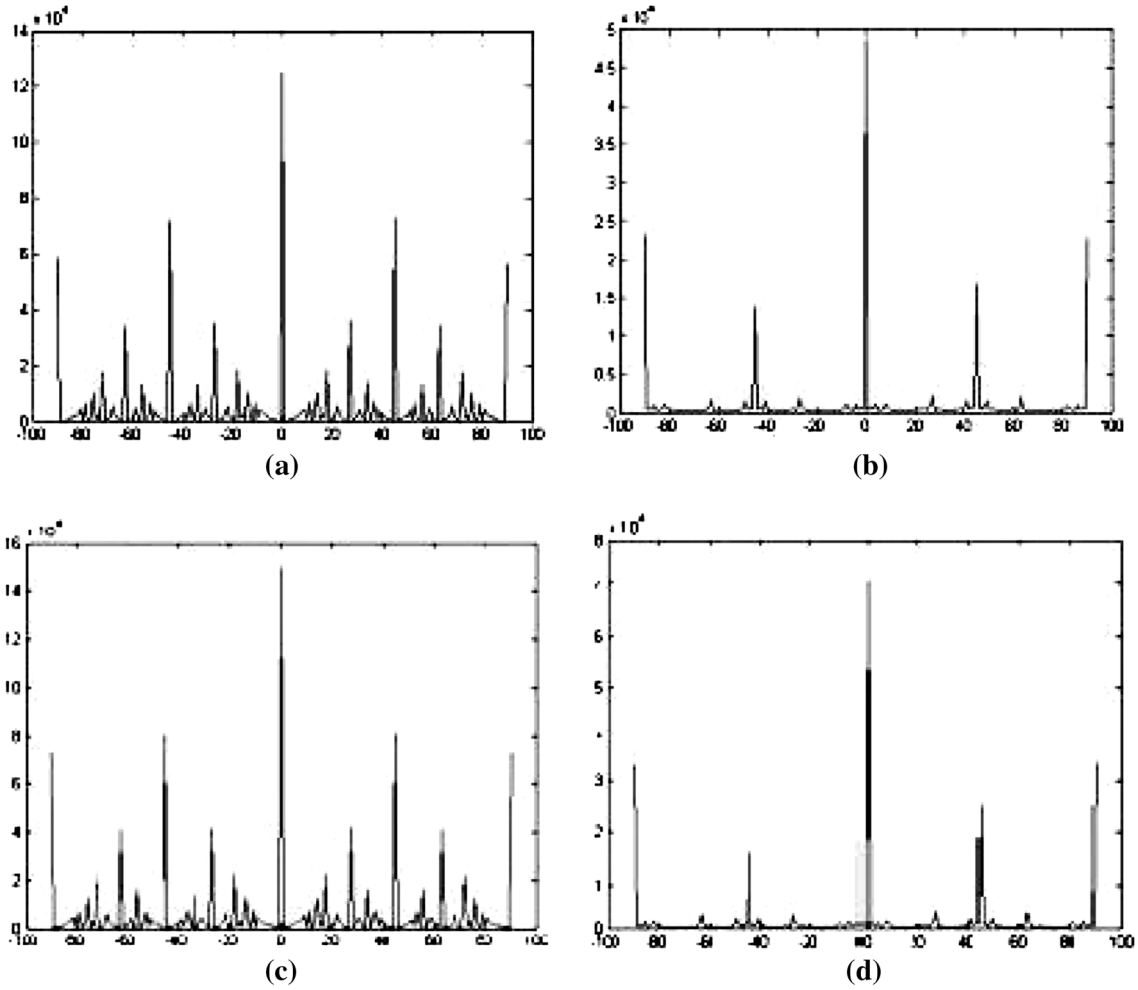

Fig. 2 Orientation histograms: **a** of an image from DRIVE database, **b** of the vesselness filter output of (**a**), **c** of an image from STARE database, **d** of the vesselness filter output of (**c**)

information of the blood vessels is a critical input for the automated self-adaptive design of the proposed modified matched filter and is unique to a particular input image. The kernel of the matched filter is modeled as a linear combination of five prominent minimally overlapping Gaussian functions in the orientation histogram. The parameters (mean, standard deviation) of these Gaussian functions as well as the weights of the linear combination (gains) are directly estimated from the orientation histogram in an automated fashion. Since these parameters have different values for different input images, the matched filter is self-adaptive for each particular input. Such non-linear synergistic combination of the vesselness filter and the matched filter using vessel orientations is, thus, far not reported for retinal blood vessel detection to the best of our knowledge.

In addition to [8,13–15], the results of the proposed method are also compared with several other well-known approaches [16–22]. In [16], Jiang and Mojon used an adaptive thresholding-based vessel segmentation algorithm. Al-Diri et al. [17] proposed a two-stage approach for vessel segmentation. The first stage comprises of a morphological filter and the second stage uses a neural cost function to resolve junction configurations. In [20], the authors proposed a multi-scale vessel segmentation algorithm using line tracking. Kaba et al., in [21], have proposed a vessel extraction scheme utilizing probabilistic modeling and expectation maximization. In [22], Bankhead et al. have used wavelets and edge location refinement to develop a retinal vessel segmentation methodology. Note that none of the methods in [16,17,20–22] employ any form of learning. Staal et al. [18] utilized supervised learning and proposed a ridge-based vessel segmentation technique employing a kNN-based classifier. Marn et al. [19] also proposed a supervised learning method for vessel segmentation utilizing moment invariants-based features. Additional comparisons with [18] and [19] further emphasize the strength of the proposed strategy.

Therefore, our principal contribution is the use of orientation histogram of the vesselness filter output in the first phase

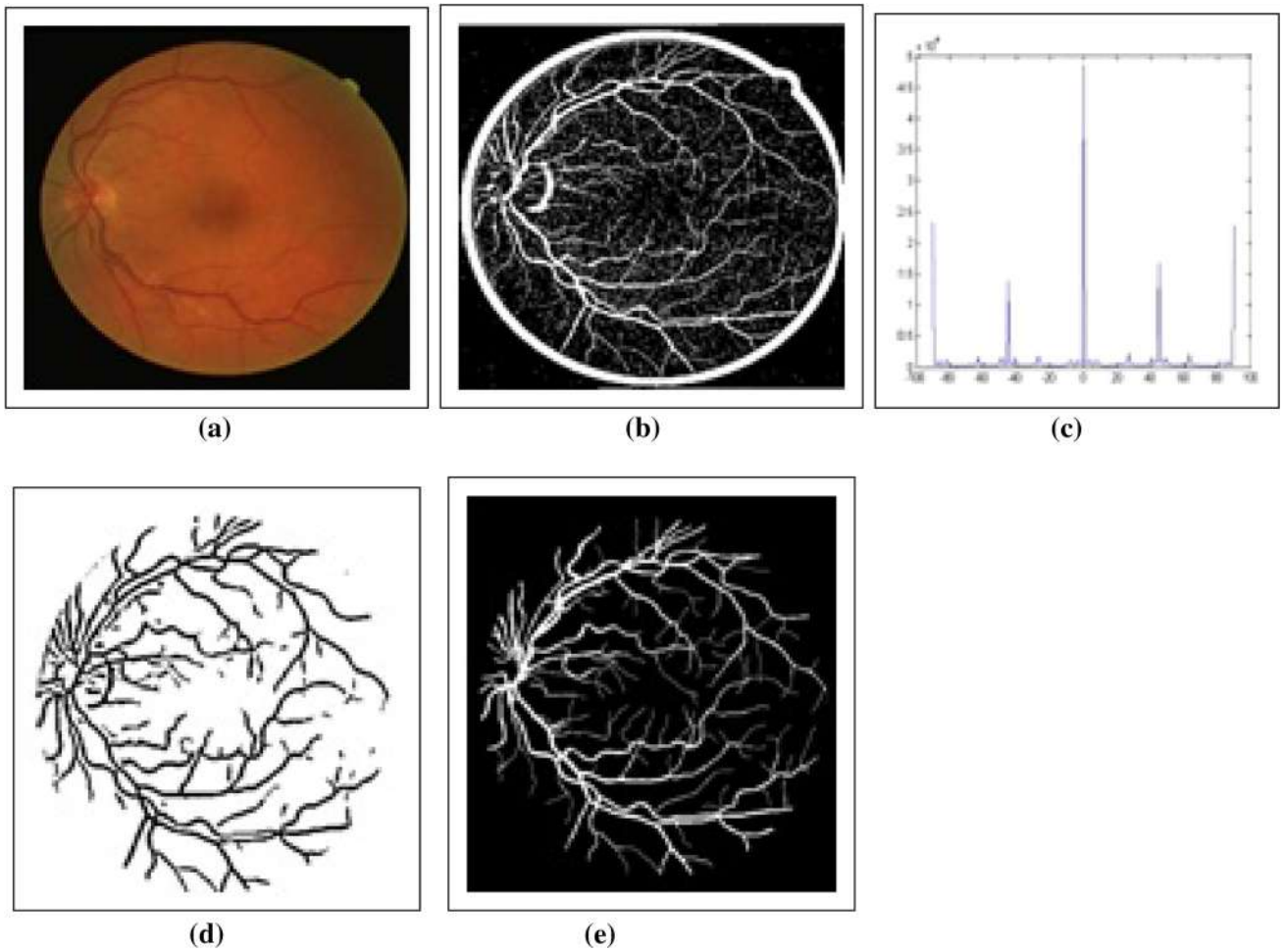

Fig. 3 Blood vessel detection using proposed method for 01_test.tif image of the DRIVE database. **a** Input image, **b** output of vesselness filter, **c** orientation histogram of (**b**), **d** final output (accuracy = 0.9302), **e** ground truth

Table 1 Parameters estimated from orientation histogram for five datasets of DRIVE database

Image	$\sigma_1 A_1$	$\sigma_2 A_2$	$\sigma_3 A_3$	$\sigma_4 A_4$	$\sigma_5 A_5$
01_test.tif	2.33, 0.4365	2.23, 0.2800	1.93, 1.00	2.13, 0.3200	2.36, 0.4327
02_test.tif	2.30, 0.4398	2.16, 0.2530	1.90, 1.00	2.10, 0.3220	2.30, 0.4403
03_test.tif	2.36, 0.4142	2.23, 0.1850	1.96, 1.00	2.16, 0.1940	2.33, 0.4145
07_test.tif	2.30, 0.4413	2.20, 0.1810	1.96, 1.00	2.10, 0.1910	2.33, 0.4435
09_test.tif	2.36, 0.4450	2.20, 0.1860	1.90, 1.00	2.13, 0.2020	2.36, 0.4439

to design the parameters of a self-adaptive matched filter in the second phase. This self-adaptive matched filter yields high sensitivity as well as high specificity thereby resulting in high accuracy. Moreover, only a single pass is required for our algorithm to complete which makes the entire process faster. Another advantage of the proposed solution is that it is completely unsupervised and hence no training set is required.

Table 2 The performance measures

Measure	Description
Specificity (Sp)	TN/(TN + FP)
Sensitivity (Sn)	TP/(TP + FN)
Accuracy (Acc)	(TP + TN)/(TP + TN + FP + FN)

3 Proposed methodology

The proposed method consists of two steps as shown below in Fig. 1. In the first step, the vesselness filter of Frangi et al. [7] is applied on the input. In the second step, a self-adaptive matched filter is designed from the orientation histogram of the output of the vesselness filter. This is achieved by estimating the parameters of the matched filter kernel by extracting relevant information present in the orientation histogram. This matched filter is applied on the output of the vesselness filter.

3.1 Vesselness filter

Detecting structures in an image based on the eigenvalues of the Hessian matrix is a well-established procedure. Frangi et al. [7] designed a multi-scale vessel enhancement filter based on the above principle. The vesselness filter is also used in recent years by Liu et al. [23] to detect blob structures in an image. Consider a 2D Gaussian filter which can be expressed by the following equation:

$$G(x, y) = \frac{1}{\sigma\sqrt{2\pi}} e^{\frac{-x^2+y^2}{2\sigma^2}} \tag{1}$$

Now for a certain scale σ (standard deviation), the Hessian matrix $H_\sigma(x, y)$ for a pixel at (x, y) is given by:

$$H_\sigma(x, y) = \begin{pmatrix} I_{xx} & I_{xy} \\ I_{yx} & I_{yy} \end{pmatrix} \tag{2}$$

Different elements of the Hessian matrix are expressed as:

$$I_{xx} = I(x, y) * \frac{\partial^2}{\partial x^2} G(x, y) \tag{3}$$

$$I_{xy} = I_{yx} = I(x, y) * \frac{\partial^2}{\partial x \partial y} G(x, y) \tag{4}$$

$$I_{yy} = I(x, y) * \frac{\partial^2}{\partial y^2} G(x, y) \tag{5}$$

For the Eqs. (3)–(5), I denotes the input image and $'*'$ denotes convolution. The eigenvalues λ_1 and λ_2 (where $|\lambda_1| < |\lambda_2|$) of the Hessian matrix are then calculated. For a particular pixel, the vesselness value V is given by [7].

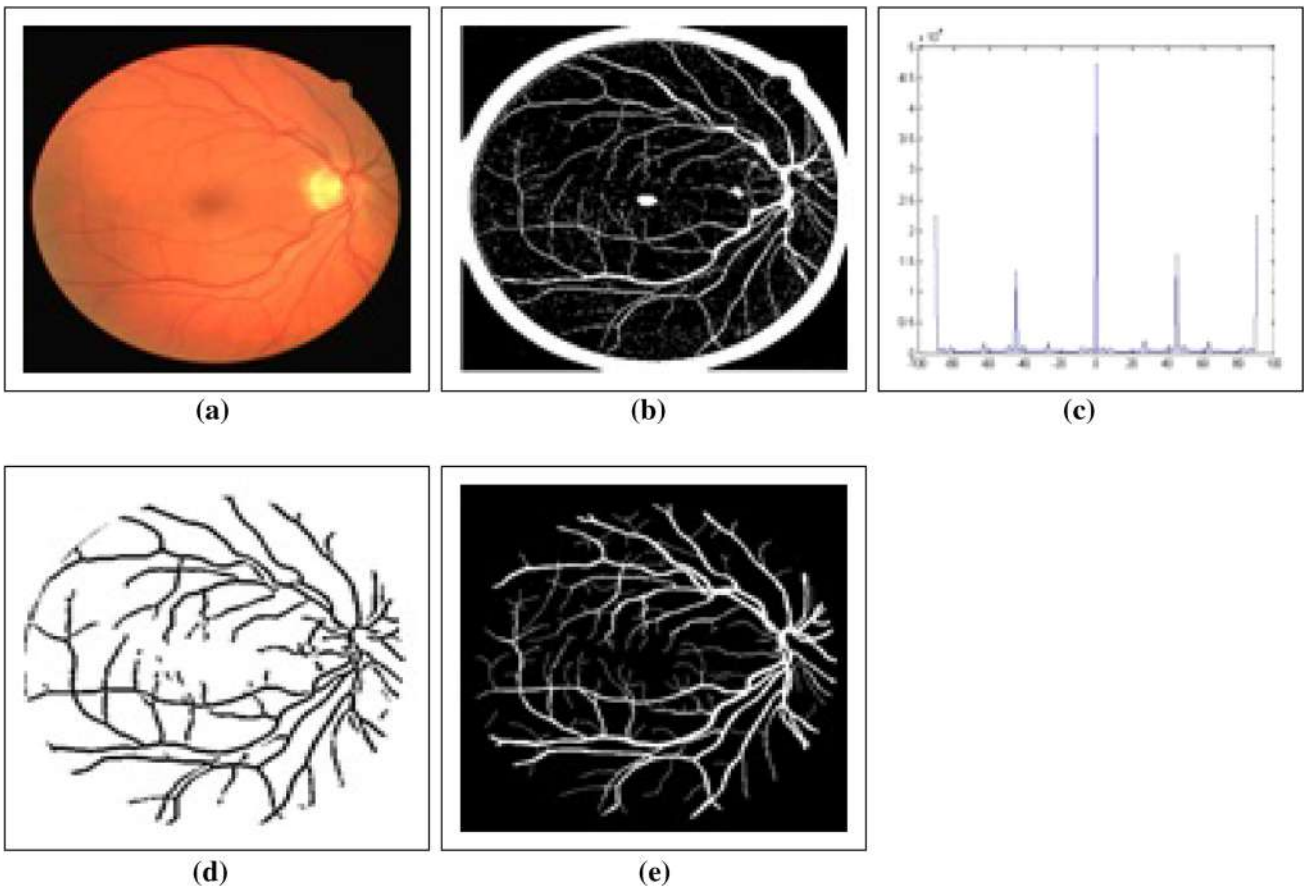

Fig. 4 Blood vessel detection using proposed method for 02_test.tif image of the DRIVE database. **a** Input image, **b** output of vesselness filter, **c** orientation histogram of (**b**), **d** final output (accuracy = 0.9421), **e** ground truth

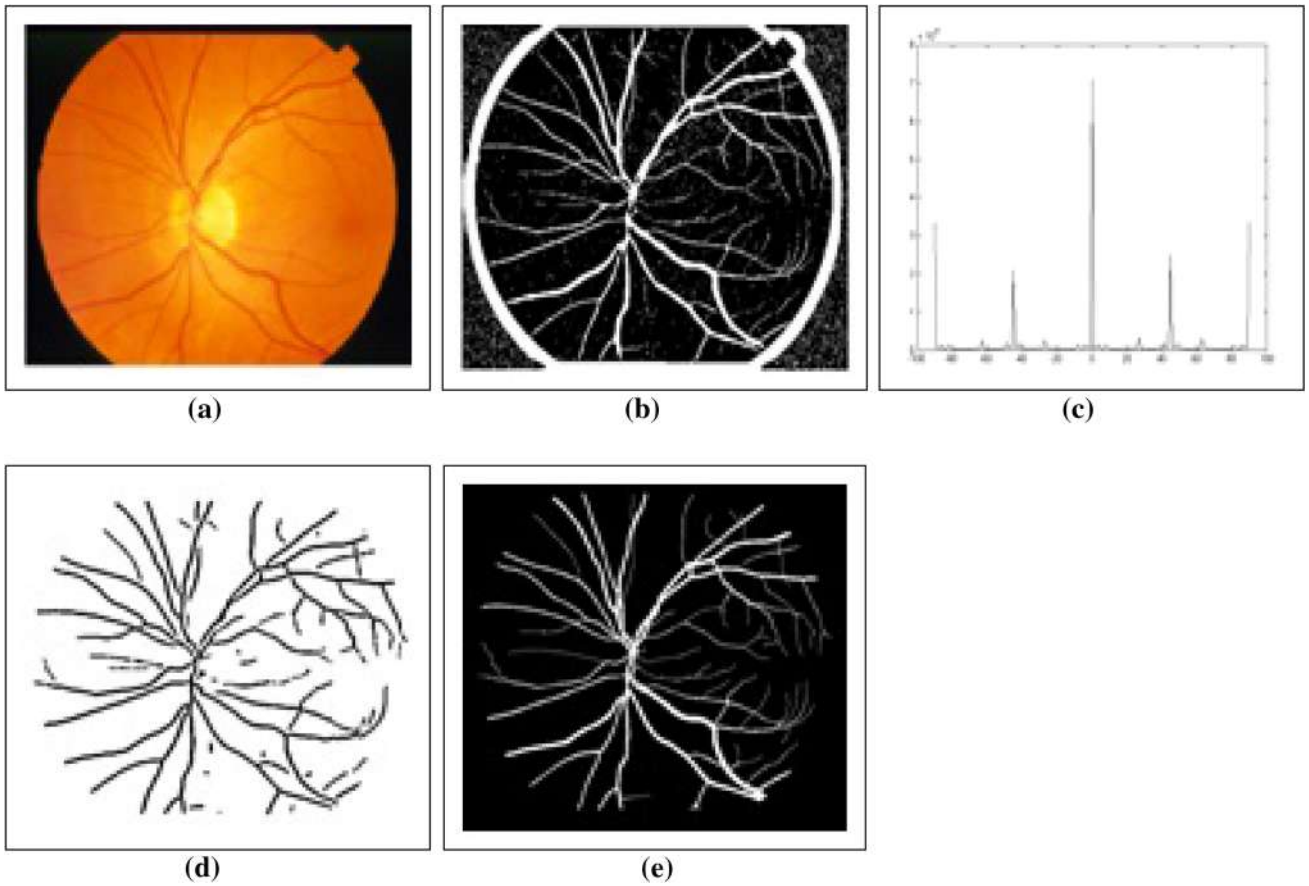

Fig. 5 Blood vessel detection using proposed method for im0163.ppm image of the STARE database. **a** Input image, **b** output of vesselness filter, **c** orientation histogram of (**b**), **d** final output (accuracy = 0.9491), **e** ground truth

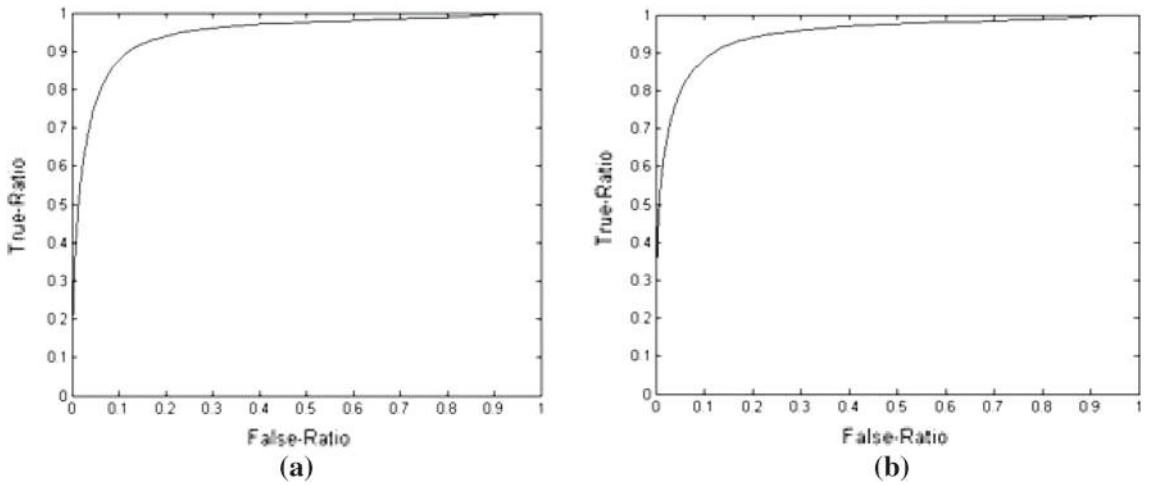

Fig. 6 ROC curve for DRIVE database. **a** 01_test.tif (AUC = 94.53) and **b** 02_test.tif (AUC = 95.21)

$$V = \begin{cases} 0, & \lambda_2 < 0 \\ e^{\frac{-r^2}{2}} \times (1 - e^{\frac{-s^2}{2}}), & \text{Otherwise} \end{cases} \quad (6)$$

From (6), it is clear that $V \in [0, 1]$. The parameters r and s in (6) are given by:

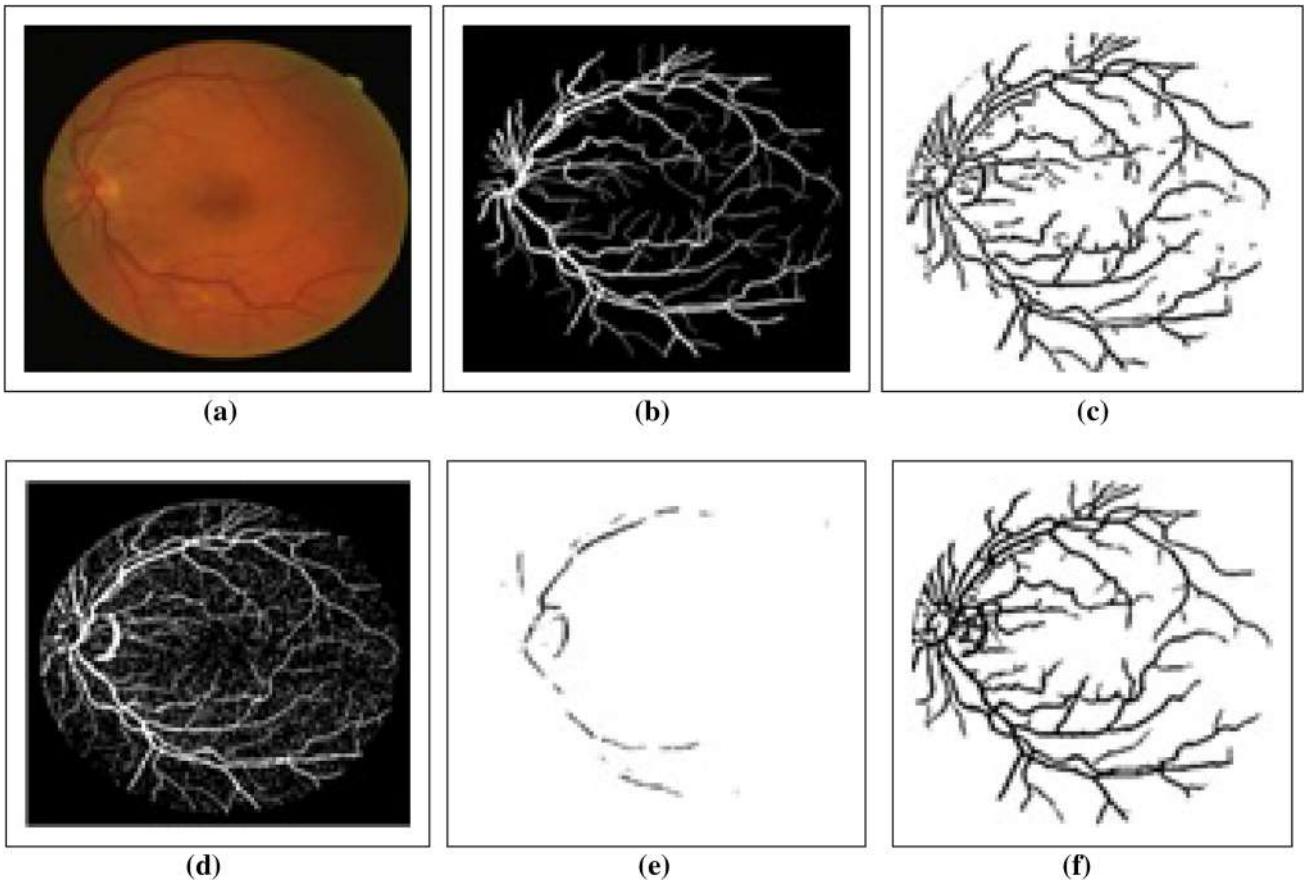

Fig. 7 Outputs of different methods for 01_test.tif image of the DRIVE database. **a** Input image, **b** ground truth image, **c** output of the proposed method (accuracy = 0.9302), **d** output of Frangi et al. [7] (accuracy = 0.9231), **e** output of Chaudhuri et al. [8] (accuracy = 0.9170), **f** output of Chanwimaluang and Fan [13] (accuracy = 0.9295)

$$r = \frac{|\lambda_1|}{|\lambda_2|} \tag{7}$$

$$s = \sqrt{(\lambda_1)^2 + (\lambda_2)^2} \tag{8}$$

3.2 Orientation histogram

The output image of the vesselness filter tends to have a high sensitivity and low specificity as shown experimentally in Sect. 4. The proposed methodology overcomes this inherent drawback by applying a matched filter, which is designed from the orientation histogram of the vesselness filter output. The matched filter kernel uses orientation angle of each pixel by rotating the kernel through small angles and noting the maximum match. The orientations of the vasculature play an important role which has not been explored thus far. An intensity histogram will not suffice in this case because different input images with differing vasculature orientations have more-or-less similar intensity profiles. Note that since the vesselness parameter lies within [0, 1], the vesselness output needs to be scaled (e.g., to [0, 255] considering a 8-bit intensity resolution) to generate a 'vesselness image'. From now on, by vesselness filter output, a vesselness image in the range [0, 255] is implied unless otherwise specified. The orientation histogram of the vesselness grayscale output and not its binary version is used next. This is because the orientation histogram retains the complete orientation information of all pixels, which would have been otherwise lost due to binarization. To construct the orientation histogram [24], the orientation angle at each pixel is calculated. For each pixel at (x, y) of the vesselness filter output image I_1, we can write:

$$\mathrm{d}y = I_1(x, y+1) - I_1(x, y-1) \tag{9}$$

$$\mathrm{d}x = I_1(x+1, y) - I_1(x-1, y) \tag{10}$$

$$\theta(x, y) = \arctan\left(\frac{\mathrm{d}y}{\mathrm{d}x}\right) \tag{11}$$

For a perfectly binary (say n-bit) image, each pixel has an intensity value of either 0 or 2^{n-1}. Thus, the difference in intensity between two pixels can be one of $\{0, -2^{n-1}$ and $2^{n-1}\}$. Hence, from Eq. (11), the orientation angle belongs to the set $\{-90°, -45°, 0°, 45°, 90°\}$. Since the orientation histogram plots the number of pixels against the orientation angles, for a perfectly binary image the orientation histogram

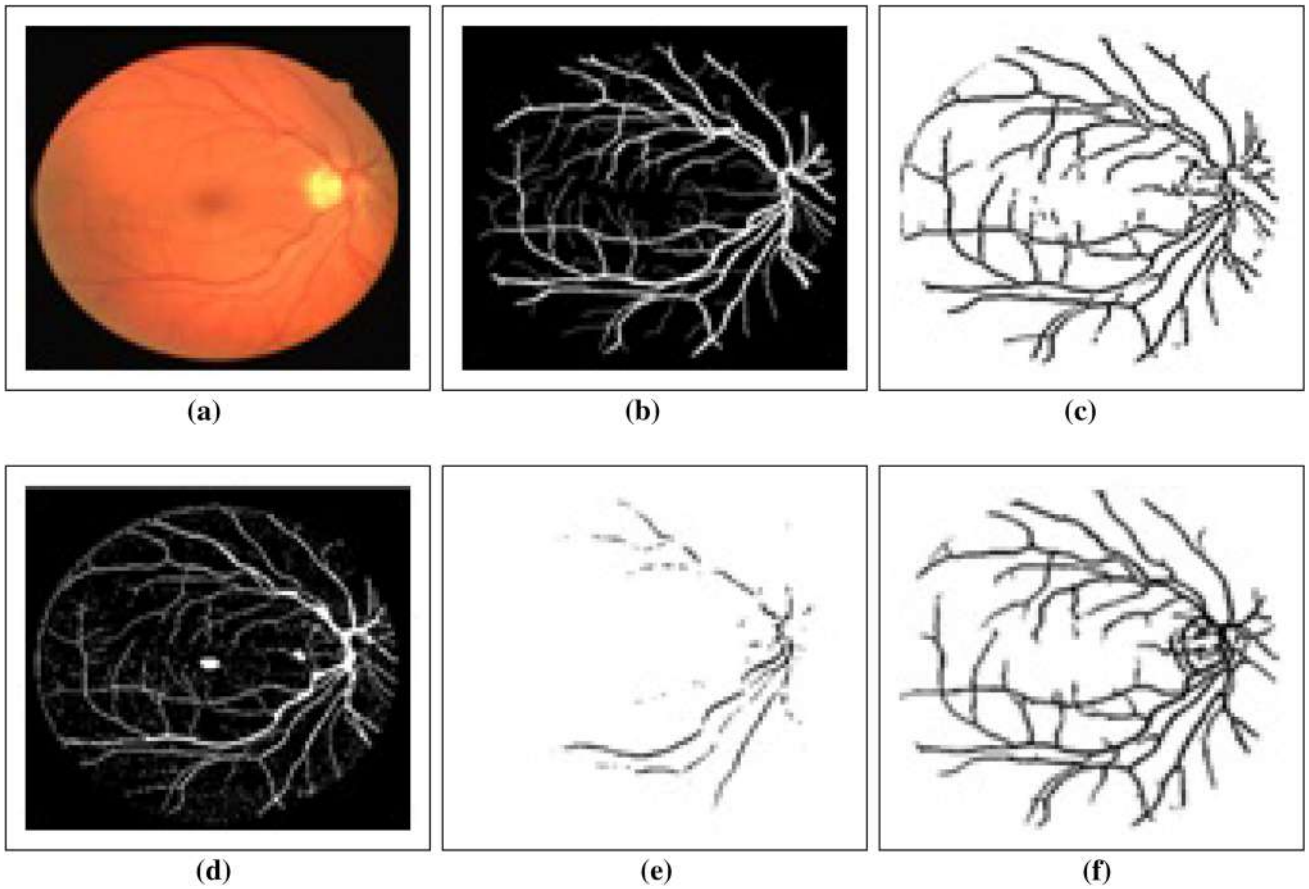

Fig. 8 Outputs of different methods for 02_test.tif image of the DRIVE database. **a** Input image, **b** ground truth image, **c** output of the proposed method (accuracy = 0.9421), **d** output of Frangi et al. [7] (accuracy = 0.9204), **e** output of Chaudhuri et al. [8] (accuracy = 0.9105), **f** output of Chanwimaluang and Fan [13] (accuracy = 0.9360)

must necessarily give impulses at the above five angles only. If the output of the vesselness filter closely resembles that of a binary image, then we can expect to find five minimally overlapping Gaussians with means at the above set of angles (see Fig. 2b, d). It is imperative that the closer an image is to being binary, the lesser will be the width or the variance of the Gaussians and hence the lesser will be the extent of overlap. This is precisely why the original input retinal image (which is far from being binary) does not generate minimally overlapping Gaussians in its orientation histogram (see Fig. 2a from DRIVE and Fig. 2c from STARE). Since the vesselness filter enhances the retinal vessels, the orientation histogram of its output consists of minimally overlapping Gaussians. Therefore, it becomes much more convenient to automatically extract the parameters of the Gaussians from the orientation histogram of the output of the vesselness filter.

3.3 Design of self-adaptive matched filter

The matched filter was originally proposed by Chaudhuri et al. [8] for the retinal blood vessel detection. Several modifications to [8] have been suggested over the years for improved detection [13–15]. The matched filter consists of a kernel, which is rotated in different directions and is matched with the input image. The principle advantage of the matched filter is its capability of removing noise resulting in high specificity. The matched filter kernel is designed as a zero mean Gaussian with unity gain [8]:

$$K(x, y) = \mathrm{e}^{\frac{-x^2}{2\sigma^2}} \quad \text{for} \quad |y| \leq \frac{L}{2} \tag{12}$$

Here, L denotes the length for which the vessel has fixed orientation. The authors have used the same value of $L = 9$ as used in other related works [8,13,14], and [15]. The kernel in Eq. (12) is rotated with an angular resolution of 15° over the range $[-90°, +90°]$, i.e., in 12 spans using the standard rotation matrix. In the available literature, only a single Gaussian function centered at 0° with a manually chosen sigma was used [8,13–15]. But the orientation histogram of the vesselness output, developed in Sect. 3.2, suggests that the kernel is actually a linear combination of five minimally overlapping Gaus-

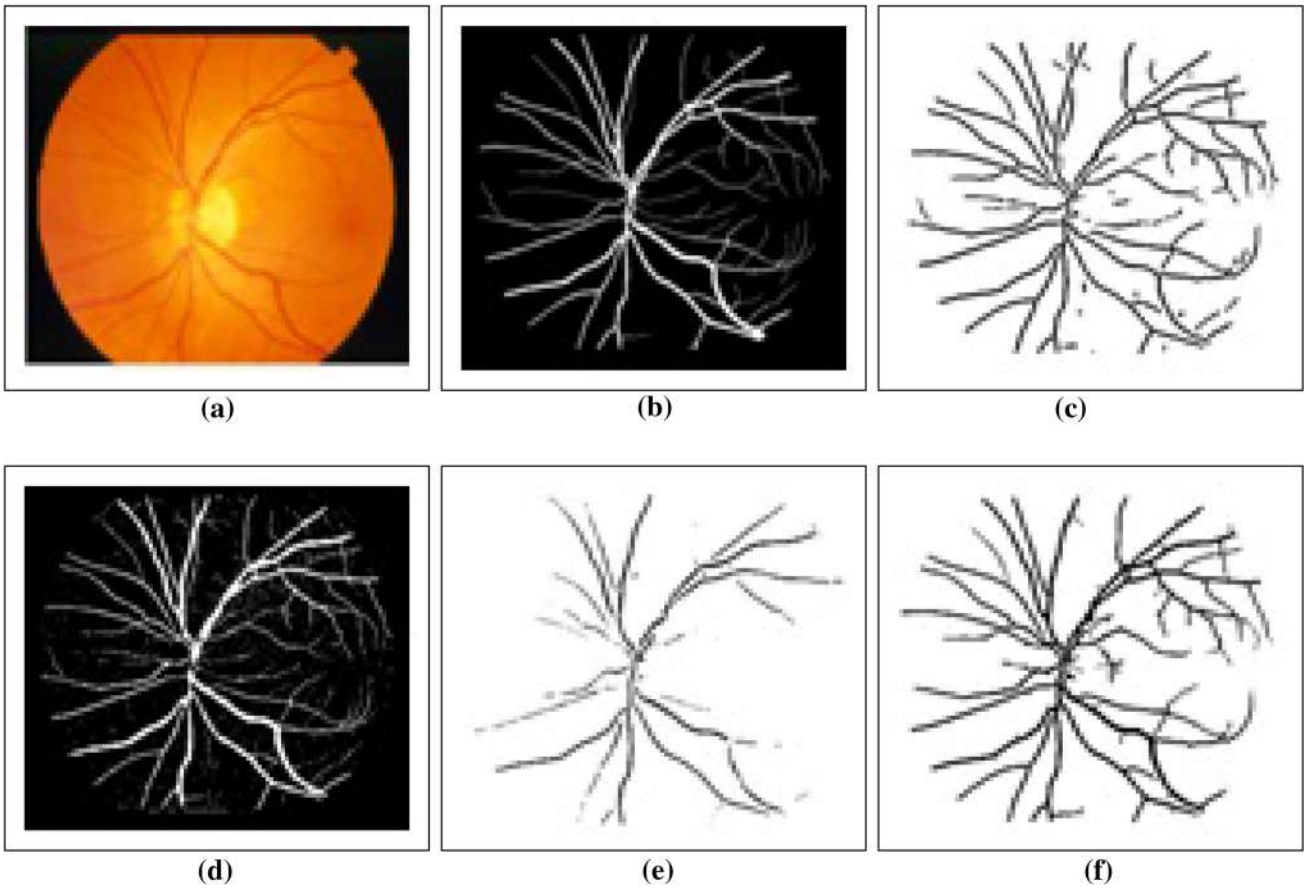

Fig. 9 Outputs of different methods for im0163.ppm image of the STARE database. **a** Input image, **b** ground truth image, **c** output of the proposed method (accuracy = 0.9491), **d** output of Frangi et al. [7] (accuracy = 0.9208), **e** output of Chaudhuri et al. [8] (accuracy = 0.9122), **f** output of Chanwimaluang and Fan [13] (accuracy = 0.9449)

sians. Thus, the modified matched filter kernel is expressed as:

$$K(x, y) = \sum_{i=1}^{5} A_i e^{-\frac{(x-\mu_i)^2}{2\sigma_i^2}} \quad \text{for} \quad |y| \leq \frac{L}{2} \tag{13}$$

In Eq. (13), A_i, μ_i and σ_i (i = 1–5) are the gains, means and standard deviations of the five Gaussian kernels. The gains and standard deviations of each of these Gaussians can be directly computed from the orientation histogram. The means of the Gaussians are already determined as −90°, −45°, 0°, 45° and 90°. The gains of the Gaussians are the normalized peak values at the above five angles as the height of the most significant Gaussian (centered at 0°) is made unity. To find the standard deviations, one standard property of the Gaussian distributions is used which states that the area under the Gaussian curve is 99.7 % at the $\pm 3\sigma$ deviation from the mean. Pixel count from the orientation histogram with a low bin width (0.1° for the present application) gives a more accurate approximation of standard deviation (sigma) of the five Gaussians. If the bin width were chosen as 1° instead, only integer values of sigma would have resulted. This is an improvement inherent in the proposed method as related works indicate use of only integer values for sigma [8,13–15].

4 Experimental results

In this work, extensive experimentations are performed on all three publicly available retinal image databases, namely, DRIVE, STARE and CHASE. Thorough qualitative as well as quantitative comparisons are done.

The DRIVE (Digital Retinal Images for Vessel Extraction) database (http://www.isi.uu.nl/Research/Databases/DRIVE/) consists of 40 color fundus photographs divided into 20 training and 20 test images [18,25]. Altogether 400 diabetic subjects between 25 and 90 years of age are studied from which 40 photographs have been randomly selected and categorized as test and training set. For each image, a mask image is provided that delineates the FOV. Furthermore, ground truths for all the 40 images are avail-

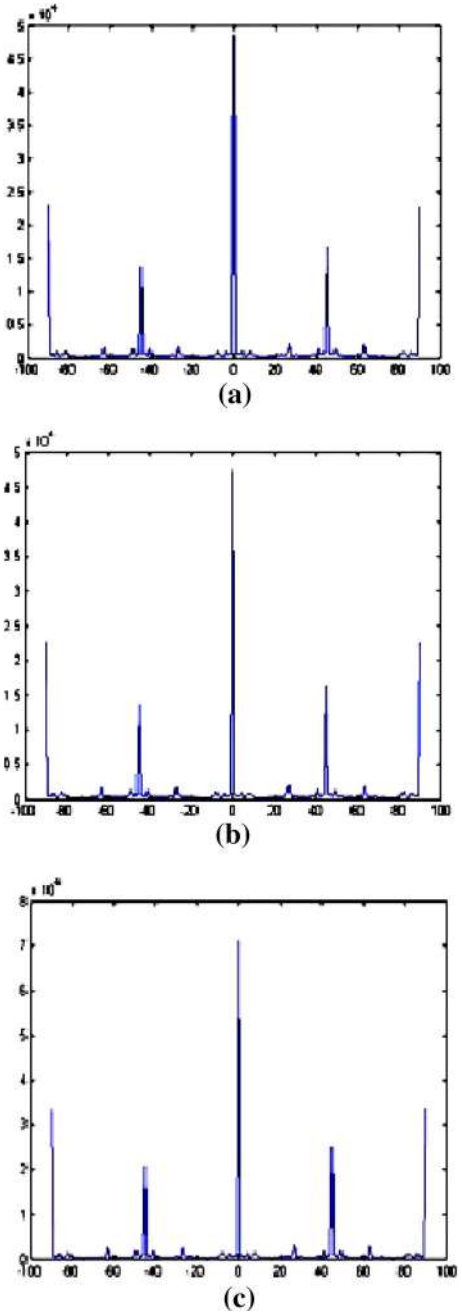

Fig. 10 Magnified orientation histogram of the output of vesselness filter for **a** 01_test.tif of DRIVE database, **b** 02_test.tif of DRIVE database, **c** im0163.ppm of STARE database

able. In this work, experiments are performed on all the 40 images (as the proposed algorithm does not require a separate training phase). The STructured Analysis of the REtina (STARE) database (http://www.parl.clemson.edu/~ahoover/stare/index.html) contains 400 images, among which the ground truths of only 20 retinal images (chosen randomly) are publicly available [26,27]. Ten out of these 20 images contain considerable pathologies making the vessel detection very challenging. Two sets of ground truth images are available for these images. Additional experimentations are also done on the recently published Child Heart and Health Studies in England (CHASE) database [28]. In this database, retinal fundus images of both eyes of each of 14 subjects are provided. Thus there are 28 input images in total, and for each input image, two ground truth images are included.

The authors first demonstrate the importance of using five Gaussians in the kernel of the matched filter. The estimated parameters from the orientation histogram for five datasets of DRIVE database are presented in Table 1.

This table clearly shows that the sigma values for the five Gaussians are quite different. For example, for the first dataset, the minimum value of sigma is 1.93 and the maximum value of sigma is 2.36 indicating more than 22 % variation. Similarly, for the second dataset, minimum value of sigma is 1.90 and the maximum value of sigma is 2.30 indicating around 21 % variation. Furthermore, the non-zero gains of all the Gaussians clearly suggest that working with a single Gaussian certainly leads to certain loss of information. For example, for the last dataset in Table 1, the other four Gaussians at $-90°$, $-45°$, $45°$, $90°$ contain 44.5, 18.60, 20.20 and 44.39 % of the total number of pixels within the main Gaussian.

For the evaluation of the proposed algorithm, accuracy (Acc), specificity (Sp) and sensitivity (Sn) are used as performance measures (see Table 2). These measures are functions of true positive (TP), true negative (TN), false positive (FP), and false negative (FN) [9,29].

The above three performance indicators are measured for the proposed method for 40 datasets of DRIVE, 20 datasets of STARE, and 28 datasets of CHASE database and the average value is used for comparison with other methods. The average execution time of our algorithm (implemented in MATLAB [30]) is approximately 8 s in a PC having Intel i3-2350M processor with speed 2.3 GHz.

The authors now present the results of blood vessel detection at different stages of the proposed method for two different images of DRIVE database (Figs. 3, 4) and one image of STARE database (Fig. 5). For better illustration, the orientation histograms obtained in Figs. 3c, 4c and 5c are presented in a more magnified form in Fig. 6a–c, respectively. All the figures clearly indicate that the outputs of the vesselness filters (Figs. 3b, 4b, 5b) are highly improved after finally applying the matched filter (Figs. 3c, 4c, 5c). The noise present in the outputs of the vesselness filter is also minimized by the matched filter.

The input image, the ground truth and the final output images (obtained by the proposed method and three competing methods are shown next in Figs. 7 and 8 (DRIVE database) and in Fig. 9 (STARE database). The binary output of [7] is obtained by first removing the outer rim from

Table 3 Performance comparison on DRIVE database

Method	Specificity (SP)	Sensitivity (SN)	Accuracy (Acc)
Frangi et al. [7]	0.6537	0.9134	0.9095
Chaudhuri et al. [8]	0.9901	0.2663	0.8773
Chanwimaluang and Fan [13]	0.9585	0.6604	0.9321
Zhang et al. [14]	0.9724	0.7120	0.9382
Jiang-Mojon [16]	0.9662	0.6363	0.9212
Cinsdikici and Aydin [15]	–	–	0.9293
Al-Diri et al. [17]	0.9551	0.7282	0.9258
Staal et al. [18]	0.9796	0.7345	0.9441
Marn et al. [19]	0.9801	0.7067	0.9452
Martinez-Perez et al. [32]	0.9655	0.7246	0.9344
Vlachos- Dermatas [20]	0.929	0.747	0.955
Frangi et al. [7] + Chaudhuri et al. [8]	0.9505	0.6565	0.9270
Kaba et al. [21]	0.9672	0.7619	0.9410
Bankhead et al. [22]	0.9717	0.7027	0.9371
Our method	0.9579	0.7205	0.9370

the vesselness filter output and then applying MATLAB's in-built thresholding function on it. All the figures clearly show that the segmentation results of the proposed method (Figs. 7c, 8c, 9c) far outweigh the results of the vesselness filter (Figs. 7d, 8d, 9d) and the matched filter (Figs. 7e, 8e, 9e). The pair of images in Figs. 7c–f and 8c–f also suggests that the results of the proposed scheme are definitely better than that of [13]. The accuracy values in the Figs. 7, 8 and 9 also conform to the visual observations.

In Table 3, the results of the proposed method is compared with several existing approaches on DRIVE [7–9,13–22,29,31,32]. In Table 4, comparisons of results on STARE are provided [7,9,14,16–19,21,29,31,32]. Since this paper does not use learning, comparison is made mostly with unsupervised techniques. In addition, to check how the proposed method performs in comparison with methods which do use learning, the results of Staal et al. [18] and Marn et al. [19] are incorporated in Table 3. Lastly, to highlight the strength of the synergistic non-linear combination of [7] and [8] using orientation histogram, results from a straightforward cascade of [7] and [8] (without the use of orientation histogram) are also included. Some of the performance measure values in Table 3 and Table 4 are taken from [1,29,31]. Table 3 shows that the proposed algorithm outperforms several recent challenging methods except [18,19,21,22]. Among these, the methods developed in [18] and [19] are supervised whereas the proposed methodology in this paper is unsupervised. The results achieved in [22] is quite comparable (almost equal accuracy, lower sensitivity and higher specificity) to those of the proposed scheme. The algorithm in [21] outperforms the proposed method in terms of accuracy, specificity, and sensitivity. However, this method uses an expectation maximization strategy where number of components needs to be specified apriori and also the process is sensitive to initialization [33]. The results in Tables 3, 4 and 5 further indicate that specificity of the proposed method is better than that of [7] and the sensitivity of the proposed method is higher than that of [8] on all three databases. The non-linear hybrid manner in which [7] and [8] are combined using the orientation histogram also proves to be decisive as this method yields higher sensitivity, specificity and accuracy compared to a direct cascading of [7] and [8]. In order to demonstrate that the improvement in accuracy obtained from our method is statistically significant as compared to several competing approaches, we further run paired t tests [34].

Note that the t test can be applied, only if the results of individual images are available for the concerned methods. Paired t test between our method and [13] (code available via (http://www.vcipl.okstate.edu/localentropy.htm) shows that the null hypothesis may be rejected with value of $p = 1.55 \times 10^{-2}$. Since our method uses both the vesselness filter [7] and the matched filter [8] as two integral components, we decide to run a paired t test on our method and each of them. Paired t test between our approach and [8] shows that the null hypothesis may be rejected with $p = 7.53 \times 10^{-7}$. Similarly, the paired t test between the proposed method and [7] suggests that the null hypothesis may be rejected with $p = 2.66 \times 10^{-9}$. The above two results clearly demonstrate that the performance of the proposed method is statistically better than that of its two integral components, [7,8]. Since the proposed method introduces an orientation histogram-based combination of the methods in [7] and [8], we also

Table 4 Performance comparison on STARE Database

Method	Specificity (SP)	Sensitivity (SN)	Accuracy(Acc)
Frangi et al. [7]	0.6625	0.8990	0.8853
Chaudhuri et al. [8]	0.9873	0.2846	0.9142
Zhang et al. [14]	0.9753	0.7177	0.9484
Jiang-Mojon [16]	–	–	0.9337
Al-Diri et al. [17]	0.9681	0.7521	–
Staal et al. [18]	–	–	0.9516
Marn et al. [19]	0.9819	0.6944	0.9526
Martinez-Perez et al. [32]	0.9569	0.7506	0.9410
Frangi et al. [7] + Chaudhuri et al. [8]	0.9516	0.6248	0.9262
Kaba et al.	0.9683	0.7466	0.9456
Our method	0.9586	0.6786	0.9379

Table 5 Performance comparison on CHASE Database

Method	Specificity (SP)	Sensitivity (SN)	Accuracy (Acc)
Frangi et al. [7]	0.6634	0.8971	0.9201
Chaudhuri et al. [8]	0.9266	0.2822	0.8487
Chanwimaluang and Fan [13]	0.9438	0.5084	0.9133
Frangi et al. [7] + Chaudhuri et al. [8]	0.9405	0.5006	0.9042
Our method (1st observer)	0.9594	0.5286	0.9298
Our method (2nd observer)	0.9583	0.5372	0.9304

Table 6 AUC for different methods over DRIVE database

Method	AUC
Chaudhuri et al. [8]	0.7878
Jiang-Mojon [16]	0.9114
Staal et al. [18]	0.9520
Marn et al. [19]	0.9588
Proposed method	0.9419

undertake a paired t test between our method and a simple cascade of [7] and [8]. Paired t test in this case indicates that the null hypothesis may be rejected with $p = 2.98 \times 10^{-9}$. Therefore, we can conclude that the proposed matched filter, whose kernel is based on the orientation histogram of the vesselness filter, yields statistically significant improvements over that of a simple cascade of the vesselness filter and the matched filter. Thus, though the absolute increments in accuracy values of the proposed method over comparable recent methods are modest, many improvements are shown to be statistically significant.

Finally to further demonstrate the robustness of the proposed method, the receiver operating curve (ROC) [12] on the DRIVE database is presented. By varying the intensity threshold value between 0 and 1 in steps of 0.001 for converting the grayscale output into binary, the corresponding true ratio is plotted against the false ratio over the range of 0–1. The resulting ROC curve is shown in Fig. 10. Here, true ratio is defined as the ratio of the true positives to the total number of vessel pixels in ground truth, and false ratio is defined as the ratio of the false positives to the total number of non-vessel pixels in the ground truth. The average area under the curve (AUC), thus, obtained for all the images of the DRIVE database is found to be 94.19 % of the maximum possible area. Table 6 shows that the AUC of the proposed method is highly comparable/better than several popular methods, except [18] and [19] which employ learning.

5 Conclusion

In this paper, a novel self-adaptive matched filter using a non-linear synergistic combination of the vesselness filter and the matched filter for the detection of retinal blood vessels is presented. Orientation histogram of the vesselness filter's output is judiciously used in an automated fashion to achieve the above synergism. This orientation histogram is found to consist of five prominent minimally overlapping Gaussian curves. The kernel of the matched filter is modeled as a linear combination of the above Gaussians, and the corresponding parameters are automatically extracted from

the orientation histogram. The matched filter with this appropriately designed kernel, when applied on the output of the vesselness filter, detects the retinal blood vessels with very high accuracy. Comprehensive experimentations show that our method outperforms several state-of-the-art retinal blood vessels detection methods and is comparable with others. One direction of future research will be to improve the sensitivity of the proposed method, especially for more complex database such as CHASE. We also plan to apply the proposed synergistic combination for detection of other similar structures like coronary blood vessel [35].

References

1. Kanski, J.J.: Clinical Ophthalmology, 6th edn. Elsevier Health Sciences, London (2007)
2. Zhang, M.: Blood vessel detection in retinal images and its application in diabetic retinopathy screening. Ph.D. Thesis, Texas A & M University (2008)
3. Rao, K.P.: Detection of Blood Vessel in the Retina Image. Oakland University, USA (2006)
4. Mirsharifa, Q., Tajeripoura, F., Pourreza, H.: Automated characterization of blood vessels as arteries and veins in retinal images. Comput. Med. Imaging Graphics **37**, 607–617 (2013)
5. Gegundez-Arias, M.E., Marin, D., Bravo, J.M., Suero, A.: Locating the fovea center position in digital fundus images using thresholding and feature extraction techniques. Comput. Med. Imaging Graphics **37**, 386–393 (2013)
6. Rothaus, K., Rhiem, P., Jiang, X.: Separation of the retinal vascular graph in arteries and veins upon structural knowledge. Image Vision Comput. **27**(7), 864–875 (2009)
7. Frangi, A., Niessen, W., Vincken, K., Viergever, M.: Multiscale vessel enhancement filtering. In: Wells, W., Colchester, A., Delp, S. (eds.) 1994, Medical Image Computing and Computer-Assisted Intervention MICCAI'98, Lecture Notes in Computer Science, vol. 1496, pp. 130–137. Springer, Berlin (1998)
8. Chaudhuri, S., Chatterjee, S., Katz, N., Nelson, M., Goldbaum, M.: Detection of blood vessels in retinal images using two-dimensional matched filters. IEEE Trans. Med. Imag. **8**, 263–269 (1989)
9. Fraz, M.M., Remagnino, P., Uyyanonvara, B., Rudnicka, A.R., Owen, C.G., Barman, S.A.: Blood vessel segmentation methodologies in retinal images a survey. Computer Methods Progr. Biomed. **108**, 407–433 (2012)
10. Kirbas, C., Quek, F.: A review of vessel extraction techniques and algorithms. ACM Comput. Surv. **36**, 81–121 (2004)
11. ZAlpaydin, E.: Introduction to Machine Learning, 2nd edn. MIT Press, USA (2010)
12. Al-Rawi, M., Qutaishat, M., Arrar, M.: An improved matched filter for blood vessel detection of digital retinal images. Computers Biol. Med. **37**, 262–267 (2007)
13. Chanwimaluang, T., Fan, G.: An efficient blood vessel detection algorithm for retinal images using local entropy thresholding. In: Proceedings, pp. 21–24. IEEE International Symposium on Circuits and Systems, Bangkok (2003)
14. Zhang, B., Zhang, L., Zhang, L., Karray, F.: Retinal vessel extraction by matched filter with first-order derivative of Gaussian. Computers Biol. Med. **40**, 438–445 (2010)
15. Cinsdikici, M.G., Aydin, D.: Detection of blood vessels in ophthalmoscope images using MF/ant (matched filter/ant colony) algorithm. Computer Methods Progr. Biomed. **96**, 85–95 (2009)
16. Jiang, X., Mojon, D.: Adaptive local thresholding by verification based multithreshold probing with application to vessel detection in retinal images. IEEE Trans. Pattern Recogn. Anal. Mach. Intell. **25**, 131–137 (2003)
17. Al-Diri, B., Hunter, A., Steel, D.: An active contour model for segmenting and measuring retinal vessels. IEEE Trans. Med. Imaging. **28**, 1488–1497 (2009)
18. Staal, J., Abramoff, M., Niemeijer, M., Viergever, M., Van Ginneken, B.: Ridge-based vessel segmentation in color images of the retina. IEEE Trans. Med. Imag. **23**, 501–509 (2004)
19. Marn, D., Aquino, A., Gegundez-Arias, M.E., Bravo, J.M.: A new supervised method for blood vessel segmentation in retinal images by using gray-level and moment invariants-based features. IEEE Trans. Med. Imaging. **30**, 146–158 (2011)
20. Vlachos, M., Dermatas, E.: Multi-scale retinal vessel segmentation using line tracking. Comput. Med. Imaging Graphics **34**, 213–227 (2010)
21. Kaba, D., Wang, C., Li Y., Salazar-Gonzalez, A., Liu X., Serag A.: Retinal blood vessels extraction using probabilistic modelling. In: Health Information Science and Systems (2014)
22. Bankhead, P., Scholfield, C.N., McGeown, J.G., Curtis, T.M.: Fast retinal vessel detection and measurement using wavelets and edge location refinement. PLoS One **7**(3), 1–12 (2012)
23. Liu, J., White, J.M., Summers, R.M.: Automated detection of blob structures by hessian analysis and object scale. In: Proceedings of IEEE International Conference on Image Processing, pp. 841–844 (2010)
24. Marimon, D., Ebrahimi, T.: Orientation histogram-based matching for region tracking. IEEE International Workshop on Image Analysis for Multimedia Interactive Services (2007)
25. Niemeijer, M., Staal, J.J., Van Ginneken, B., Loog, M., Abramoff, M.D.: Comparative study of retinal vessel segmentation methods on a new publicly available database. SPIE Med. Imaging. **5370**, 648–656 (2004)
26. Hoover, A., Kouznetsova, V., Goldbaum, M.: Locating blood vessels in retinal images by piece-wise threhsold probing of a matched filter response. IEEE Trans. Med. Imaging. **19**, 203–210 (2000)
27. Hoover, A., Goldbaum, M.: Locating the optic nerve in a retinal image using the fuzzy convergence of the blood vessels. IEEE Trans. Med. Imaging **22**, 951–958 (2003)
28. Fraz, M., Remagnino, P., Hoppe, A., Uyyanonvara, B., Rudnicka, A.R., Owen, C.G., Barman, S.A.: An ensemble classification-based approach applied to retinal blood vessel segmentation. IEEE TBME **59**(9), 2538–2548 (2012)
29. Villalobos-Castaldi, F., Felipe-Riveron, E., Sanchez-Fernandez, L.: A fast, efficient and automated method to extract vessels from fundus images. J. Vis. **13**, 263–270 (2010)
30. MATLAB 2011b, The MathWorks Inc., Natick, MA, USA. www.mathworks.com
31. Fraz, M.M., Barman, S.A., Remagnino, P., Hoppe, A., Basit, A., Uyyanonvara, B., Rudnicka, A.R., Owen, C.G.: An approach to localize the retinal blood vessels using bit planes and centerline detection. Computer Methods Progr. Biomed. **108**(2), 600–616 (2012)
32. Martinez-Perez, M.E., Hughes, A.D., Thom, S.A., Bharath, A.A., Parker, K.H.: Segmentation of blood vessels from red-free and fluorescein retinal images. Med. Image Anal. **11**, 47–61 (2007)
33. Abd-Almageed, W., El-Osery, A., Smith, C. E.: Non-parametric expectation maximization: a learning automata approach. In: IEEE Proceedings of Int. Conf. System, Man and Cybernetics, Washington D.C., pp. 1–6 (2003)
34. Demsar, J.: Statistical comparisons of classifiers over multiple data sets. J. Mach. Learn. Res. **7**, 1–30 (2006)
35. Zifan, A., Chapman, B.E.: Automatic detection of coronary vessels using mutli-scale texture dictionaries. In: Proceedings of IEEE International Conference on Healthcare Informatics, p. 115 (2012)

Tapabrata Chakraborti completed his BEng and MEng from Jadavpur University, India. His research interests are in the fields of digital image processing, biometrics, biomedical image analysis, pattern recognition and machine learning. He is currently working as Assistant Engineer in the Government of his State.

Dhiraj K. Jha completed his MEng from Jadavpur University and is currently teaching in the Electrical and Electronics Engineering Department in Swami Vivekananda Institute of Science and Technology, Kolkata, India. His research interests are in medical image processing, pattern recognition and embedded systems design.

Ananda S. Chowdhury received a B.Sc. (Hons.) in Physics from Presidency University, India in 1996, a B.Tech in Electronics Engineering from the Institute of Radiophysics and Electronics, India in 1999, and an M.E. in Computer Engineering from Jadavpur University, India in 2001. He earned his Ph.D. in Computer Science from the University of Georgia, USA in July 2007. From August 2007 to December 2008, he worked as a postdoctoral fellow in the Department of Radiology and Imaging Sciences at the National Institutes of Health, USA. Currently, he is working as an Associate Professor in the Department of Electronics and Telecommunication Engineering at Jadavpur University, India. His research interests include computer vision, pattern recognition and biomedical image processing. He is a member of the IEEE, the IEEE Computer Society, the IEEE Signal Processing Society and the IAPR. His Erdős number is 2.

Xiaoyi Jiang studied Computer Science at Peking University and received his Ph.D. and Venia Docendi (Habilitation) degree in Computer Science from University of Bern, Switzerland. He was an Associate Professor at Technical University of Berlin, Germany. Since 2002, he is a professor of Computer Science at University of Münster, Germany. Currently, he is Editor-in-Chief of Int. Journal of Pattern Recognition and Artificial Intelligence and also serves on the advisory board and editorial board of several journals including Pattern Recognition, IEEE Transactions on Cybernetics, and Chinese Science Bulletin. His research interests include biomedical image analysis, 3D image analysis, and structural pattern recognition. He is a PI of the new Cluster of Excellence "Cells in Motion" http://www.uni-muenster.de/CiMIC/ funded by the German Excellence Initiative. He is Senior Member of IEEE and Fellow of IAPR.